Measurement of $\pi^- p \to \eta n$ from threshold to $p_{\pi^-} = 747$ MeV/c

S. Prakhov,[1] B. M. K. Nefkens,[1] C. E. Allgower,[2,*] R. A. Arndt,[3] V. Bekrenev,[4] W. J. Briscoe,[3] M. Clajus,[1] J. R. Comfort,[5] K. Craig,[5] D. Grosnick,[6] D. Isenhower,[7] N. Knecht,[8] D. Koetke,[6] A. Koulbardis,[4] N. Kozlenko,[4] S. Kruglov,[4] G. Lolos,[8] I. Lopatin,[4] D. M. Manley,[9] R. Manweiler,[6] A. Marušić,[1,†] S. McDonald,[1,‡] J. Olmsted,[9,§] Z. Papandreou,[8] D. Peaslee,[10] N. Phaisangittisakul,[1] J. W. Price,[1] A. F. Ramirez,[5] M. Sadler,[7] A. Shafi,[3] H. Spinka,[2] T. D. S. Stanislaus,[6] A. Starostin,[1] H. M. Staudenmaier,[11] I. I. Strakovsky,[3] I. Supek,[12] W. B. Tippens,[1,¶] and R. L. Workman[3]
(Crystal Ball Collaboration)
[1]*University of California Los Angeles, Los Angeles, California 90095-1547, USA*
[2]*Argonne National Laboratory, Argonne, Illinois 60439-4815, USA*
[3]*The George Washington University, Washington, D.C. 20052-0001, USA*
[4]*Petersburg Nuclear Physics Institute, Gatchina, RU-188350 Russia*
[5]*Arizona State University, Tempe, Arizona 85287-1504, USA*
[6]*Valparaiso University, Valparaiso, Indiana 46383-6493, USA*
[7]*Abilene Christian University, Abilene, Texas 79699-7963, USA*
[8]*University of Regina, Saskatchewan, Canada S4S OA2*
[9]*Kent State University, Kent, Ohio 44242-0001, USA*
[10]*University of Maryland, College Park, Maryland 20742-4111, USA*
[11]*Universität Karlsruhe, Karlsruhe, D-76128 Germany*
[12]*Rudjer Boskovic Institute, Zagreb, Croatia 10002*
(Received 6 April 2005; published 14 July 2005)

The differential cross section for η production in reaction $\pi^- p \to \eta n$ has been measured over the full angular range at seven incident π^- beam momenta from threshold to $p_{\pi^-} = 747$ MeV/c using the Crystal Ball multiphoton spectrometer. The angular distributions are S wave dominated. At 10 MeV/c above threshold, a small D-wave contribution appears that interferes with the main S wave. The total η production cross section σ^{tot} is obtained by integration of $d\sigma/d\Omega$. Starting at threshold, σ^{tot} rises rapidly, as expected for S-wave-dominated production. The features of the $\pi^- p \to \eta n$ cross section are strikingly similar to those of the SU(3) flavor-related process $K^- p \to \eta\Lambda$. Comparison of the $\pi^- p \to \eta n$ reaction is made with η photoproduction.

DOI: 10.1103/PhysRevC.72.015203 PACS number(s): 13.75.−n, 25.40.Ve, 25.80.Hp

I. INTRODUCTION

The gross features of η production near threshold in reaction

$$\pi^- p \to \eta n \tag{1}$$

were explored in early literature, but the experiments were of limited precision; they have been reviewed in Ref. [1]. The total cross section, σ^{tot}, rises rapidly immediately from threshold. The magnitude of σ^{tot} at $p_{\pi^-} = 720$ MeV/c, which is just 35 MeV/c above threshold, was found to be around 2 mb, which is surprisingly large. Phase space favors $\sigma^{\text{tot}}(\pi^- p \to \pi^0 n)$ by a factor of six at $p_{\pi^-} = 740$ MeV/c, whereas experimentally $\sigma^{\text{tot}}(\pi^- p \to \pi^0 n) = 2.5 \cdot \sigma^{\text{tot}}(\pi^- p \to \eta n)$ around that momentum. We even find that $\sigma^{\text{tot}}(\pi^- p \to \eta n) > \sigma^{\text{tot}}(\pi^- p \to \pi^0\pi^0 n)$ from $p_{\pi^-} = 720$ MeV/c to $p_{\pi^-} = 750$ MeV/c [2]. Early measurements of the differential cross section were of poor quality, with low statistics and at limited angular intervals.

We report here the results of new, extensive measurements of $d\sigma/d\Omega$ using the Crystal Ball (CB) multiphoton spectrometer. This detector covers 93% of the full solid angle. It allows two simultaneous measurements of η production over the complete angular region using the two principal decay modes of the η meson: $\eta \to \gamma\gamma$ and $\eta \to 3\pi^0$; it enables us to make a significant check on the Monte Carlo (MC) evaluation of the CB acceptance, as $d\sigma/d\Omega$ must be the same for the two decay modes.

η mesons are produced predominantly via the $N(1535)\frac{1}{2}^-$ intermediate state. When incorporated into a partial-wave analysis (PWA), we anticipate that our new data will help to improve the evaluation of the mass, width, and decay branching ratios of this baryon resonance. There is a more-than-average interest in the properties of the $N(1535)\frac{1}{2}^-$ because it is believed to be the chiral partner of the nucleon ground state [3]. The mass of the $N(1535)$ is only a few hundred mega-electron-volts below the proposed onset of chiral restoration.

It is of interest to compare the features of η production by π^- and K^-, specifically reaction (1) and

$$K^- p \to \eta\Lambda, \tag{2}$$

*Present address: Midwest Proton Radiotherapy Institute, 2425 Milo B. Sampson Ln., Bloomington, IN 47408.
†Present address: Collider-Accelerator Dept., Brookhaven National Laboratory, Upton, NY 11973.
‡Present address: TRIUMF, 4004 Wesbrook Mall, Vanccouver, B.C., Canada V6T 2A3.
§Present address: Physics and Computer Planning, 810 Ingraham Pl., Charlotte, NC 28270.
¶Present address: Nuclear Physics Div., Dept. of Energy, 19901 Germantown Road, Germantown, MD 20874-1290.

measured earlier with the Crystal Ball [4]. Naively, one might expect these two reactions to be quite different. The initial $\pi^- p$ state in reaction (1) has only u and d quarks, whereas the $K^- p$ state in reaction (2) has also the s quark of the incident K^- meson that is transferred in the η-production process to the outgoing Λ baryon. Experimentally, there were early indications [5] of a remarkable similarity in the features of η production near threshold by π^- and K^-. This is now understood as a manifestation of SU(3) flavor symmetry of massless quarks. Apparently when the quarks have mass, the flavor symmetry is broken but not destroyed.

Extensive data exist on η photoproduction [6], with more to come from MAinz MIcrotron (MAMI), Electron Stretch Accelerator (ELSA), and Jefferson Lab (JLab). So it is natural to make a comparison of η production by π^- and γ. η photoproduction is an electromagnetic interaction and does not exhibit flavor symmetry. However, η production by both π^- and γ is dominated by the $N(1535)$ intermediate state. We venture that the total cross section has a similar dependence on the η momentum in the center of mass (c.m.), whereas the shape of the angular distribution should be quite different. Photoproduction involves the vector mesons ρ, ω, and ϕ, whereas η production by π^- does not [7].

II. EXPERIMENTAL SETUP

The measurements of $\pi^- p \to \eta n$ were performed at Brookhaven National Laboratory with the Crystal Ball multiphoton spectrometer installed in the C6 beam line of the Alternating Gradient Synchrotron. The Crystal Ball consists of 672 optically isolated NaI(Tl) crystals, shaped like truncated triangular pyramids and arranged in two hemispheres that cover 93% of 4π steradians. The typical energy resolution for electromagnetic showers in the CB was $\Delta E/E = 0.020/(E[\mathrm{GeV}])^{0.36}$. Shower directions were measured with a resolution in the polar angle θ with respect to the beam axis of $\sigma_\theta = 2^\circ$–3° for photon energies in the range 50–500 MeV, assuming that the photons are produced in the center of the CB. The resolution in azimuthal angle ϕ is $\sigma_\theta/\sin\theta$. The experiment was performed with a momentum-analyzed beam of negative pions incident on a 10-cm-long liquid hydrogen (LH_2) target located in the center of the CB. The beam spread σ_p/p at the CB target was about 1%. The mean momentum of the beam spectrum at the target center was known to a precision of $\sim$2.5 MeV/c. The beam trigger was a coincidence between three scintillation counters located in the beam line upstream of the CB. The CB event trigger was the beam trigger in coincidence with a Crystal Ball signal, which included the requirement that the total energy deposited in the crystals exceeded a certain threshold. The neutral-event trigger required the anticoincidence of the CB event trigger with the signals from a barrel of scintillation counters surrounding the target. More details about the CB detector and the data analyses can be found in Refs. [2,4,8,9].

III. DATA HANDLING

To measure reaction $\pi^- p \to \eta n$, we used the two dominant decay modes of η to neutrals: $\eta \to 2\gamma$ and $\eta \to 3\pi^0$. The candidates for the

$$\pi^- p \to \eta n \to \gamma\gamma n \tag{3}$$

and

$$\pi^- p \to \eta n \to 3\pi^0 n \to 6\gamma n \tag{4}$$

channels are the neutral two-cluster and six-cluster events, respectively, assuming that each cluster is because of a photon shower in the CB. The neutron is assumed to be the missing particle. Because the $\pi^- p \to \eta n$ reaction is measured near the production threshold, only a few events have the final-state neutron entering the crystals of the CB (i.e., almost all events have the neutrons escaping through the downstream tunnel of the CB). At the highest momentum $p_{\pi^-} = 747$ MeV/c, the fraction of the $\pi^- p \to \eta n$ events with the neutron detected in the CB is only 4%. So in our analysis of the experimental and MC sets, we did not consider events in which there was an extra cluster from a neutron interaction in the CB.

The "cluster" algorithm was optimized for finding a group of neighboring crystals in which the energy was deposited from a single-photon electromagnetic shower. The software threshold for the cluster energy was chosen to be 14 MeV; this value optimizes the number of reconstructed $\pi^- p \to \eta n$ events.

All two- and six-cluster events were subjected to a kinematic fit to test the $\pi^- p \to \eta n \to 2\gamma n$ and $\pi^- p \to \eta n \to 6\gamma n$ hypotheses, respectively. The hypothesis on the mass of η meson was taken as $m_\eta = 547.45$ MeV. The same η mass was used for the MC simulation. The measured parameters in the kinematic fit included five for the beam particle (momentum, angles θ_x and θ_y, and position coordinates x and y in the target) and three for each photon cluster (energy, angles θ, and ϕ). Because the neutron was not observed, its energy and two angles were free parameters in the fit. The z coordinate of the vertex was also a free parameter in the kinematic fit. In addition to the four main constraints of the kinematic fit, which are based on energy and three-momentum conservation, there is one more constraint: the invariant mass of the final-state photons must have the value of the known η-meson mass. The total number of constraints for both hypotheses is five. The effective number of constraints is smaller by the number of free parameters of the fit; thus we have a 1-C fit. The pulls of the kinematic fit for the beam, photon, and neutron variables were adjusted to agree with a normal distribution that has its mean value zero and variance 1. A small deviation from the normal distribution occurs for events with a large cluster multiplicity, when some clusters overlap, or when a part of the electromagnetic shower leaks into the CB exit tunnel.

Events that satisfied the $\pi^- p \to \eta n \to 2\gamma n$ or $\pi^- p \to \eta n \to 6\gamma n$ hypothesis at the 2% confidence level (CL) (i.e., with a probability greater than 2%) were accepted as the corresponding event candidates. A tighter cut on the CL is unnecessary, as there is no physical background. The production of the $3\pi^0 n$ final state that is not from an η decay is negligibly small at these energies [9]. We neglected this contribution. The only background that occurs is η production in target material different from LH_2. The magnitude of this background was estimated using empty-target data. It comprises about 2% and was subtracted from the LH_2 spectra. In addition,

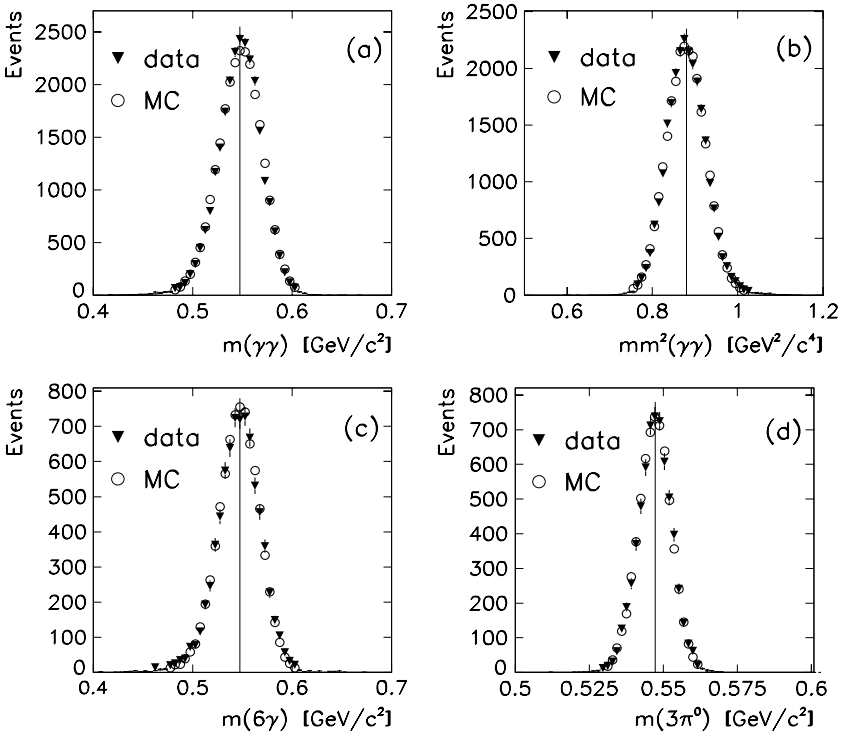

FIG. 1. Comparison of data (solid triangles) and MC (circles) distributions. For $\pi^- p \to \eta n \to \gamma\gamma n$: (a) two-photon invariant mass and (b) missing mass squared. For $\pi^- p \to \eta n \to 6\gamma n$: (c) six-photon invariant mass. For $\pi^- p \to \eta n \to 3\pi^0 n \to 6\gamma n$: (d) $3\pi^0$ invariant mass. The vertical line in (a), (c), and (d) shows the η mass. The vertical line in (b) shows the proton mass squared.

the $\eta \to 6\gamma$ events were subjected to a kinematic fit for testing the 4-C hypothesis $\pi^- p \to \eta n \to 3\pi^0 n \to 6\gamma n$ and the 3-C hypothesis $\pi^- p \to 3\pi^0 n \to 6\gamma n$. The kinematic fit was performed for each of the 15 possible pairing combination of six photons to form three π^0s. The pairing combination with the largest CL was used to reconstruct the kinematics of the process.

The actual beam spectrum extracted for $\pi^- p \to \eta n$ from the data was used as the input to a MC simulation of this reaction. Another input is the production angular distribution, which we assumed to be isotropic. The simulation of the $\eta \to 3\pi^0$ decay was made according to phase space. Next, the MC events were propagated through a full GEANT (version 3.21) simulation of the CB detector, folded with the CB resolutions and trigger conditions, and analyzed the same way as the experimental data.

The agreement between the data and the MC-simulation distributions obtained for the $\pi^- p \to \eta n$ reaction is illustrated in Fig. 1. Figure 1(a) compares the data and MC distributions for the two-photon invariant-mass spectrum obtained from two-cluster events selected as the $\pi^- p \to \eta n \to 2\gamma n$ process. For the same events, Fig. 1(b) compares the missing mass squared. In Fig. 1(c), we compare the six-photon invariant-mass spectrum for events selected as $\pi^- p \to \eta n \to 6\gamma n$. The invariant-mass resolution for the $\eta \to 2\gamma$ and $\eta \to 6\gamma$ events is $\sigma \approx 21$ MeV/c^2. Testing the $\pi^- p \to 3\pi^0 n \to 6\gamma n$ hypothesis, in which the constraint on the η-mass was omitted, illustrates the improvement in the CB invariant mass resolution because of the application of a kinematic fit. In Fig. 1(d), we compare the $3\pi^0$ invariant-mass spectra of the data and the MC simulation. Both invariant-mass spectra have $\sigma \approx$ 5 MeV/c^2. Note that the peak of the three invariant-mass spectra is in good agreement with the η mass, as well as the peak of the missing-mass-squared spectrum with the neutron mass squared.

Figure 2 illustrates the determination of the $\pi^- p \to \eta n$ differential cross section using $\eta \to \gamma\gamma$ events at a beam momentum of 732 MeV/c. In Fig. 2(a), one can see the experimental yield dependence on the η-production angle θ^* in the overall c.m. system. The empty-target yield can be seen in Fig. 2(b). The MC acceptance as a function of $\cos\theta^*$ is displayed in Fig. 2(c). The resulting differential cross section is shown in Fig. 2(d). The calculation of the number of the beam pions incident on the target and the number of the protons in the target is described in detail in Ref. [2]. The value for $BR(\eta \to \gamma\gamma)$ of $0.3949 \pm 0.0017 \pm 0.0030$ is taken from Ref. [10].

Figure 3 illustrates the determination of the $\pi^- p \to \eta n$ differential cross section using $\eta \to 3\pi^0$ events for beam momentum 732 MeV/c, with $BR(\eta \to 3\pi^0) = 0.3251 \pm 0.0029$ from Ref. [11].

IV. RESULTS

A. The differential and total cross section

The two sets of results for the differential cross section $d\sigma/d\Omega$ for reaction (1) obtained using $\eta \to 2\gamma$ and $\eta \to 3\pi^0$ decays are shown in Fig. 4. Their numerical comparison are made in the next section. Inspection of Fig. 4 reveals that the $d\sigma/d\Omega$ results obtained using $\eta \to 2\gamma$ decay is smoother than the ones obtained using $\eta \to 3\pi^0$. This can be explained by the fact that the number of $\eta \to 2\gamma$ decays detected in the CB is 3.5 times the $\eta \to 3\pi^0$ ones. Furthermore, the acceptance for $\eta \to 2\gamma$ events [see Fig. 2(c)] is quite uniform; it varies by only a factor 1.3 with $\cos\theta^*$. Meanwhile, the acceptance

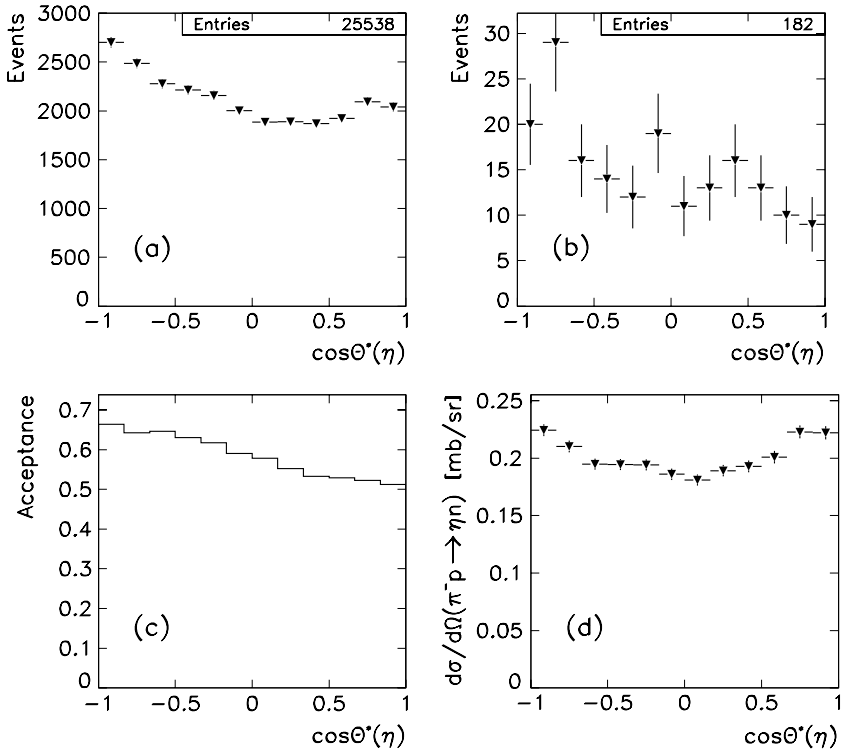

FIG. 2. Angular dependences on the η-production angle θ^* in the overall c.m. system obtained for $\eta \to \gamma\gamma$ events at beam momentum 732 MeV/c: (a) LH_2 data, (b) empty-target data, (c) MC acceptance, and (d) final differential cross section.

for $\eta \to 3\pi^0$ [see Fig. 3(c)] varies by nearly a factor of 3. Note also that the angular resolution for θ^* varies from 22° at $p_{\pi^-} = 687$ MeV/c to 8° at $p_{\pi^-} = 747$ MeV/c.

The systematic uncertainty in $d\sigma/d\Omega$ is dominated by two sources: the uncertainty in the η decay branching ratio and the uncertainty in the determination of the incident π^- beam flux. The absolute uncertainty in the value of BR($\eta \to 2\gamma$), which has been determined directly [10], is only 0.9%. In contrast, BR($\eta \to 3\pi^0$) has been determined only relatively. Thus, we prefer to use the $d\sigma/d\Omega$ data set obtained using

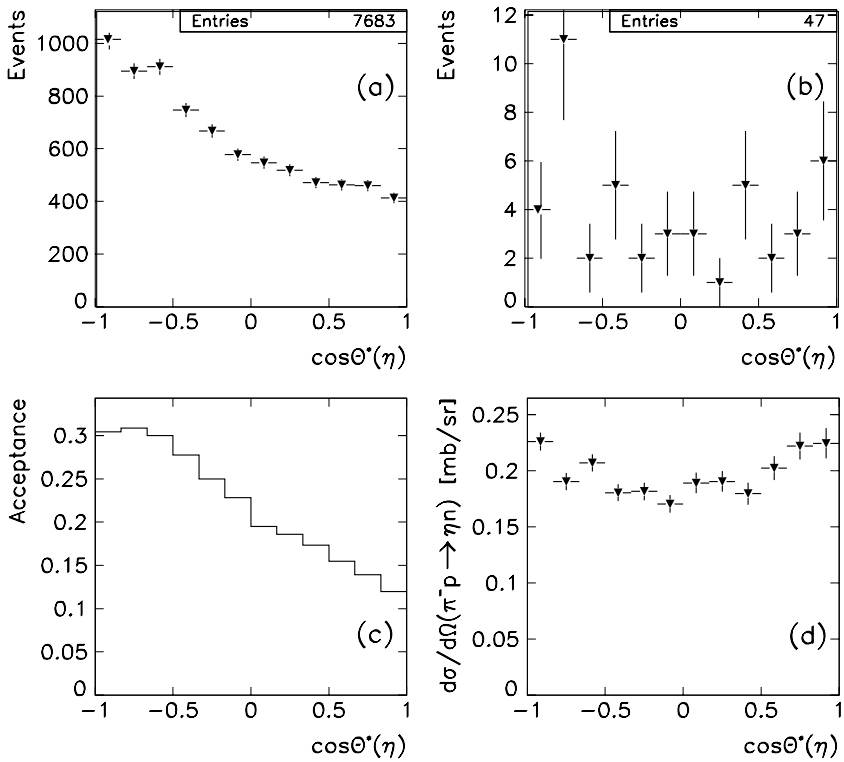

FIG. 3. Same as described in legend to Fig. 2 but for $\eta \to 3\pi^0$ events.

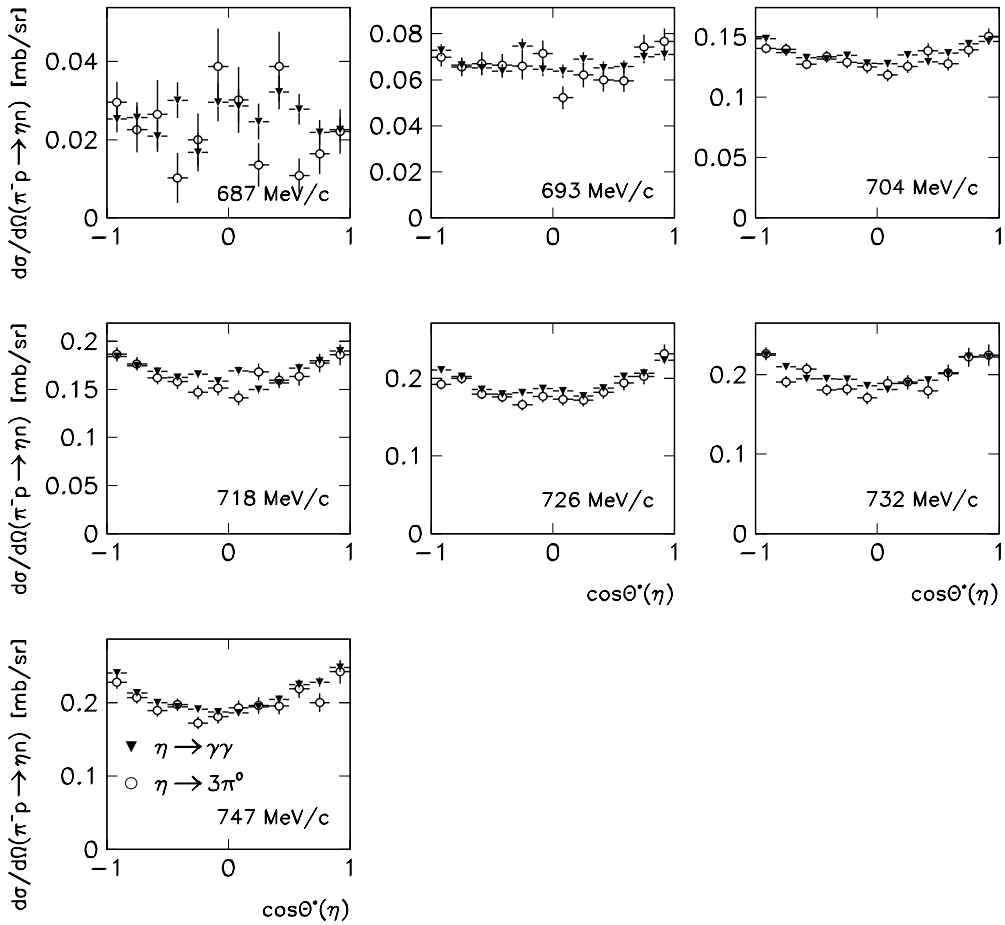

FIG. 4. Differential cross section for $\eta \to \gamma\gamma$ (filled triangles) and $\eta \to 3\pi^0$ (open circles) decays obtained at the seven-beam momenta.

$\eta \to 2\gamma$ rather than taking the weighted average of the two sets. Our numerical results for $d\sigma/d\Omega$ obtained using $\eta \to 2\gamma$ are listed in Tables I and II. Not included is the systematic uncertainty of 6% that originates in the uncertainty in our determination of the contamination of the incident π^- beam, which has been discussed in detail in Ref. [2].

The total cross section was obtained by integrating $d\sigma/d\Omega$. Values of the total cross section are listed in Tables I and II.

TABLE I. Results for the total and differential cross section for reaction $\pi^- p \to \eta n$ for the four lowest beam momenta. σ_p is the beam momentum spread for $\pi^- p \to \eta n$ events.

$p_{\pi^-} \pm \sigma_p$ (MeV/c)	687 ± 3	693 ± 5	704 ± 6	718 ± 7
σ^{tot} (mb)	0.320 ± 0.015	0.850 ± 0.010	1.711 ± 0.011	2.126 ± 0.016
$d\sigma/d\Omega$ (mb/sr)				
$\cos\theta^* = -0.92$	0.0253 ± 0.0034	0.0728 ± 0.0026	0.1486 ± 0.0029	0.1841 ± 0.0045
$\cos\theta^* = -0.75$	0.0257 ± 0.0039	0.0664 ± 0.0027	0.1372 ± 0.0029	0.1743 ± 0.0044
$\cos\theta^* = -0.58$	0.0209 ± 0.0040	0.0652 ± 0.0028	0.1329 ± 0.0028	0.1685 ± 0.0044
$\cos\theta^* = -0.42$	0.0301 ± 0.0046	0.0638 ± 0.0029	0.1317 ± 0.0028	0.1623 ± 0.0044
$\cos\theta^* = -0.25$	0.0167 ± 0.0049	0.0747 ± 0.0031	0.1349 ± 0.0029	0.1658 ± 0.0043
$\cos\theta^* = -0.08$	0.0295 ± 0.0048	0.0645 ± 0.0030	0.1283 ± 0.0029	0.1584 ± 0.0043
$\cos\theta^* = 0.08$	0.0286 ± 0.0044	0.0637 ± 0.0029	0.1277 ± 0.0029	0.1689 ± 0.0047
$\cos\theta^* = 0.25$	0.0246 ± 0.0045	0.0689 ± 0.0031	0.1353 ± 0.0030	0.1499 ± 0.0044
$\cos\theta^* = 0.42$	0.0321 ± 0.0043	0.0652 ± 0.0029	0.1293 ± 0.0029	0.1565 ± 0.0044
$\cos\theta^* = 0.58$	0.0278 ± 0.0039	0.0657 ± 0.0027	0.1369 ± 0.0030	0.1719 ± 0.0048
$\cos\theta^* = 0.75$	0.0218 ± 0.0032	0.0700 ± 0.0029	0.1443 ± 0.0031	0.1798 ± 0.0049
$\cos\theta^* = 0.92$	0.0225 ± 0.0030	0.0710 ± 0.0027	0.1464 ± 0.0031	0.1899 ± 0.0050

TABLE II. Same as Table I for the three highest beam momenta.

$p_{\pi^-} \pm \sigma_p$ (MeV/c)	726 ± 7	732 ± 6	747 ± 7
σ^{tot} (mb)	2.434 ± 0.017	2.527 ± 0.019	2.629 ± 0.021
$d\sigma/d\Omega$ (mb/sr)			
$\cos\theta^* = -0.92$	0.2105 ± 0.0045	0.2245 ± 0.0051	0.2404 ± 0.0057
$\cos\theta^* = -0.75$	0.2019 ± 0.0046	0.2101 ± 0.0051	0.2130 ± 0.0055
$\cos\theta^* = -0.58$	0.1855 ± 0.0043	0.1948 ± 0.0048	0.1996 ± 0.0051
$\cos\theta^* = -0.42$	0.1792 ± 0.0043	0.1946 ± 0.0048	0.1940 ± 0.0051
$\cos\theta^* = -0.25$	0.1814 ± 0.0043	0.1942 ± 0.0048	0.1911 ± 0.0054
$\cos\theta^* = -0.08$	0.1865 ± 0.0045	0.1861 ± 0.0049	0.1875 ± 0.0054
$\cos\theta^* = 0.08$	0.1837 ± 0.0045	0.1811 ± 0.0048	0.1858 ± 0.0054
$\cos\theta^* = 0.25$	0.1771 ± 0.0045	0.1891 ± 0.0051	0.1939 ± 0.0058
$\cos\theta^* = 0.42$	0.1869 ± 0.0047	0.1929 ± 0.0053	0.2045 ± 0.0061
$\cos\theta^* = 0.58$	0.2020 ± 0.0050	0.2009 ± 0.0053	0.2244 ± 0.0063
$\cos\theta^* = 0.75$	0.2064 ± 0.0050	0.2229 ± 0.0056	0.2280 ± 0.0064
$\cos\theta^* = 0.92$	0.2229 ± 0.0054	0.2221 ± 0.0057	0.2481 ± 0.0068

The systematic uncertainty of 6% is not included in the uncertainties in the total cross section. Preliminary results of this measurement were published some time earlier in Ref. [13].

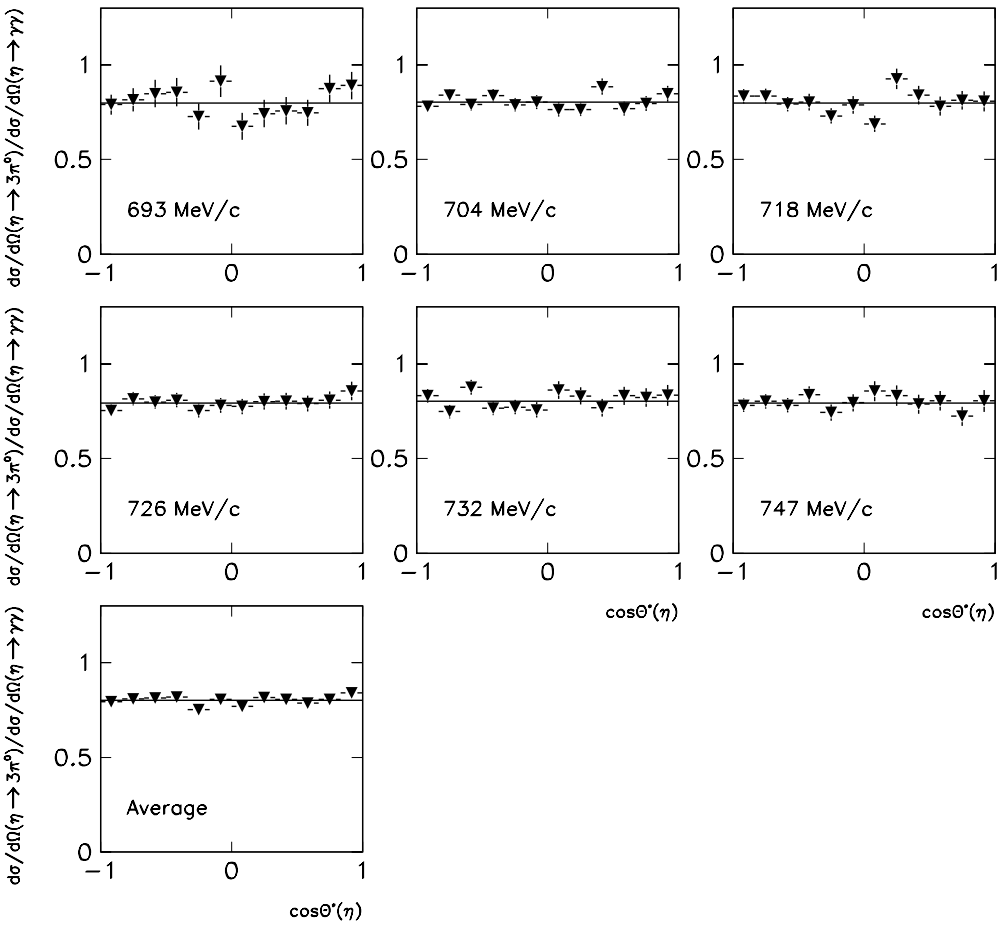

FIG. 5. Fit of the ratio $d\sigma/d\Omega(\pi^- p \to \eta n \to 3\pi^0 n)/d\sigma/d\Omega(\pi^- p \to \eta n \to 2\gamma n)$ to a constant separately for six incident π^- beam momenta and for the average ratio.

TABLE III. Results of the fit of the R ratios of Fig. 5 to a constant separately for six beam momenta and for the average of all six.

p_{π^-} (MeV/c)	R	χ^2/ndf
693	0.799 ± 0.020	11.2/11
704	0.804 ± 0.010	10.9/11
718	0.799 ± 0.013	17.5/11
726	0.791 ± 0.011	5.50/11
732	0.803 ± 0.012	13.1/11
747	0.793 ± 0.013	6.70/11
Average	0.801 ± 0.006	14.9/11

B. Comparison of the two $d\sigma/d\Omega$ data sets

To evaluate the level of agreement of the two $d\sigma/d\Omega$ data sets shown in Fig. 4, we use the ratio

$$R = \frac{d\sigma/d\Omega(\pi^- p \to \eta n \to 3\pi^0 n)}{d\sigma/d\Omega(\pi^- p \to \eta n \to 2\gamma n)}$$

that is shown in Fig. 5 for six incident π^- beam momenta as a function of $\cos\theta^*$. Not shown is the lowest energy data for lack of statistics. The seventh ratio shown in Fig. 5 is the average of the first six distributions. All angular distributions of R are fitted to a horizontal straight line. The fit value for R for each distribution is given in Table III together with the χ^2/ndf value. The latter shows that the horizontal straight line is a good description. This is a demonstration of the correctness of the MC calculation of the different acceptances for $\eta \to 2\gamma$ and $\eta \to 3\pi^0$ events.

The physical meaning of R is that it is the ratio of the two branching ratios, $R = BR(\eta \to 3\pi^0)/BR(\eta \to \gamma\gamma)$. From the fit of the average R distribution, we obtain

$$R = 0.801 \pm 0.006.$$

The value quoted by the Particle Data Group is $R_{\rm PDG} = 0.825 \pm 0.007$ [11]. The agreement of these ratios with our average value is just acceptable but not very good:

$$R_{\rm PDG}/R = 1.030 \pm 0.012$$

After completion of this work a new determination of the ratio was published by the ELSA group [12]. They quote for R the value $0.822 \pm 0.002_{\rm stat} \pm 0.004_{\rm syst}$, but no energy and angular dependence of R comparable to our Fig. 5 and Table III is provided, nor is there an evaluation of the magnitude of the background because of $\eta \to 3\pi^0$ from pure $3\pi^0$ photoproduction.

V. DISCUSSION

The results on $d\sigma/d\Omega(\pi^- p \to \eta n)$ at the seven π^- beam momenta are compared to the most recent PWA of the GW SAID group [14], which is a coupled-channel analysis of πN elastic and ηN production data. It gives an excellent description of the shape of the differential cross section. In the SAID analysis, the ηN production amplitude has a dominant S-wave component and a much smaller D_{13} amplitude that is connected to the $N^*(1520)\frac{3}{2}^-$ resonance.

First, we should deal with the effects of the uncertainty in the absolute π^- beam momentum value, which is $\sim$2.5 MeV/c, and the uncertainty in the mass of the η. The Saclay value for the η mass is 547.30 ± 0.15 MeV [17]. NA48 quotes $547.84 \pm 0.03 \pm 0.04$ MeV [18]. The difference of 0.5 MeV is equivalent to a threshold difference of 0.8 MeV/c in π^-. The effect of the uncertainty in the π^- beam momentum and the η mass value is to increase the uncertainty in the value of the η momentum in the c.m. p^*_η, especially close to threshold.

The seven angular distributions are presented in Fig. 6. The solid line is the FA02 prediction for $m_\eta = 547.3$ MeV. The effect of $\pm$2.5 MeV/c uncertainty in the π^- momentum is to raise or lower all $d\sigma/d\Omega$ by the same fraction marked by the shaded area in Fig. 6. The impact is quite large near threshold. Shown for comparison are the existing $d\sigma/d\Omega$ data selected using the criteria of Ref. [14]. Note the significant improvement in the precision of the new data.

To enable us to make an accurate comparison of the shape of our $d\sigma/d\Omega$ angular distributions with the FA02 prediction, we have normalized the FA02 result in Fig. 6 to our experimental data. From Fig. 6, we conclude that the agreement in shape is very good. The normalization factors are given in Table IV; they deviate from 1.0 by more than the 6% systematic uncertainty. This implies that the BR of $N^*(1535)\frac{1}{2}^-$ to ηN perhaps needs fine tuning.

The straightforward interpretation of our data is that η production in reaction $\pi^- p \to \eta n$ in the threshold region is dominated by S-wave production. The η angular distributions are symmetric around 90°, indicative of the absence of a P-wave contribution. The bowl shape of the angular dependence of $d\sigma/d\Omega$ is consistent with the presence of 5–10% D wave with S-D interference as discussed later [see Eq. (5) and Fig 8(b)]. It suggests that the $N(1520)\frac{3}{2}^-$ and/or $N(1675)\frac{5}{2}^-$ has a small nonzero branching into ηN. An ηN branch of 17% has been reported for $D_{15} \to \eta N$ by the η-MAID PWA [15]. Quark-model predictions by Capstick and Isgur predict negligible D_{13} decay amplitudes to ηN (+0.4 for $N(1520)\frac{3}{2}^-$ and -0.2 for $N(1700)\frac{3}{2}^-$), but a significant D_{15} decay amplitude (-2.5 for $N(1675)\frac{5}{2}^-$) [16]. Polarization experiments for the $\pi^- p \to \eta n$ reaction are needed to pin down the different D-wave contributions. Shown in Fig. 7 are the CB $d\sigma/d\Omega$ data and the unnormalized FA02 predictions.

TABLE IV. Comparison of the FA02 (which does not include our data) [14], I375, and F375 solutions with the present data. Norm is the normalization factor for each π^- momentum.

P_π (MeV/c)	χ^2/Data			Norm		
	FA02	I375	F375	FA02	I375	F375
687	2.8	3.0	2.9	1.33	1.36	1.34
693	1.4	1.3	1.4	1.01	1.04	1.08
704	3.9	2.5	1.8	0.80	0.82	0.92
718	3.5	2.0	1.9	0.89	0.91	1.04
726	1.9	1.3	1.1	0.89	0.90	1.00
732	2.2	0.9	0.7	0.92	0.94	1.00
747	0.6	0.7	1.1	1.02	1.04	0.99

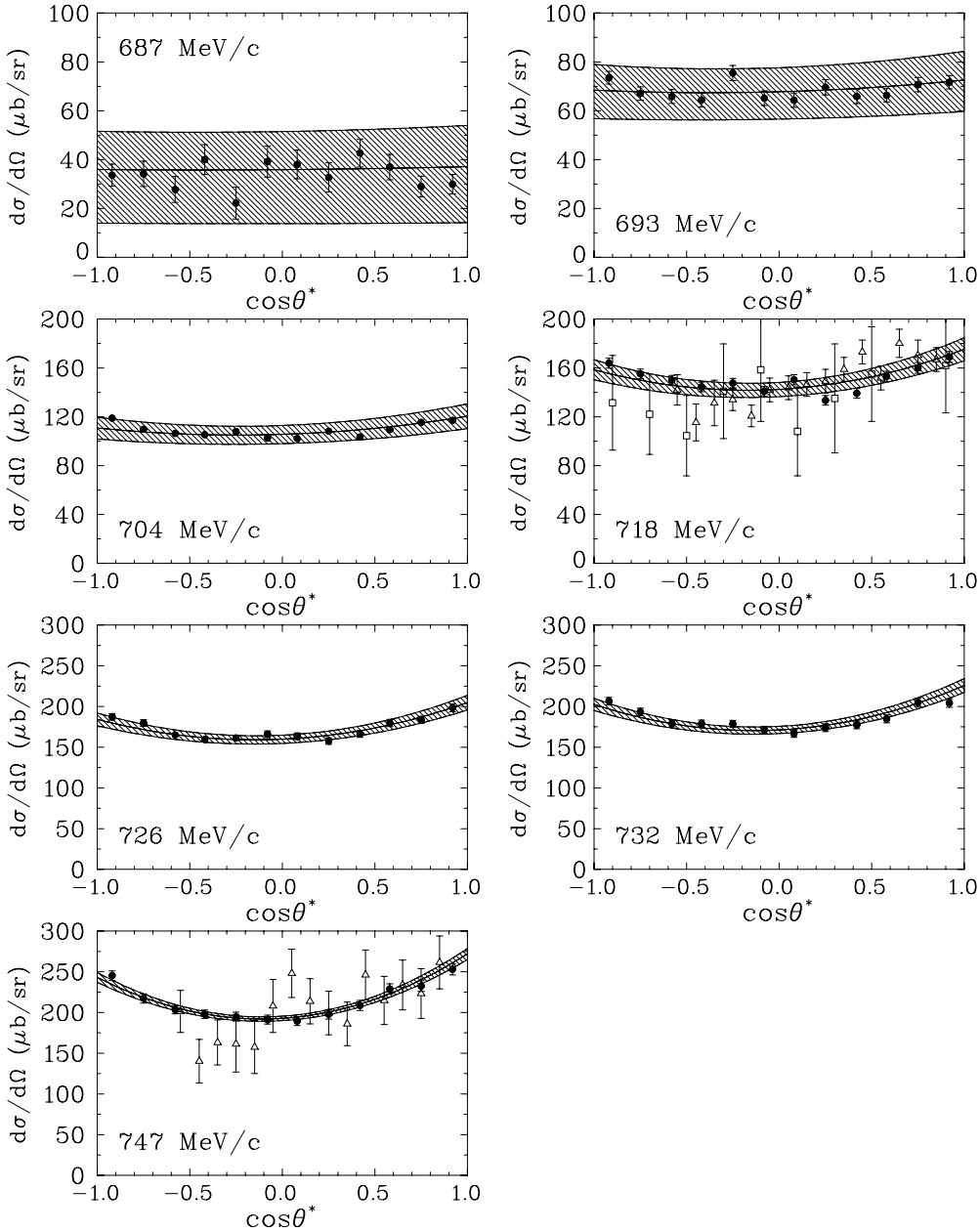

FIG. 6. Effect of ±2.5 MeV/c momentum uncertainty for $\pi^- p \to \eta n$ differential cross section for the seven incident π^- momenta. The error bars show the statistical uncertainties only. Solid lines correspond to the GW SAID FA02 solution [14]. Bands correspond to variations in the FA02 predictions for ±2.5 MeV/c. Experimental data are the current measurement (filled circles), from Ref. [19] (open triangles), and from Ref. [20] (open squares). The PWA predictions have been renormalized to the data; the normalization factors are given in Table IV.

After adding the CB results to the existing SAID data base, we have made a new PWA solution. The result is labeled I375. It is shown in Fig. 7 by a dashed line. We have also made a CB-data-weighted PWA by giving the CB data a weight factor of 5. The result for the PWA is called F375. The fit to our data looks reasonable.

We have fitted our $d\sigma/d\Omega$ data at each energy with a Legendre polynomial expansion

$$\frac{d\sigma}{d\Omega} = a_0 + a_1 P_1(\cos\theta^*) + a_2 P_2(\cos\theta^*). \qquad (5)$$

The values of the a_i coefficients are shown in Fig. 8 as a function of the π^- momentum. We consider a_i/a_0 to reduce the effect of S-wave. a_1/a_0 is consistent with zero as expected. a_2/a_0 rises rapidly above threshold at $p_{\pi^-} = 685$ MeV/c, supporting the presence of a D-wave component.

It is interesting to explore the new features of F375 PWA. This is done in Fig. 9(a) for the S_{11} partial amplitude for πN elastic scattering and in Fig. 9(b) for D_{13}.

Finally an evaluation is made in Fig. 10(a) of the S_{11} amplitude for $\pi^- N \to \eta N$; it indicates that the S_{11} mass implied by F375 could be smaller than for I375, in an extreme

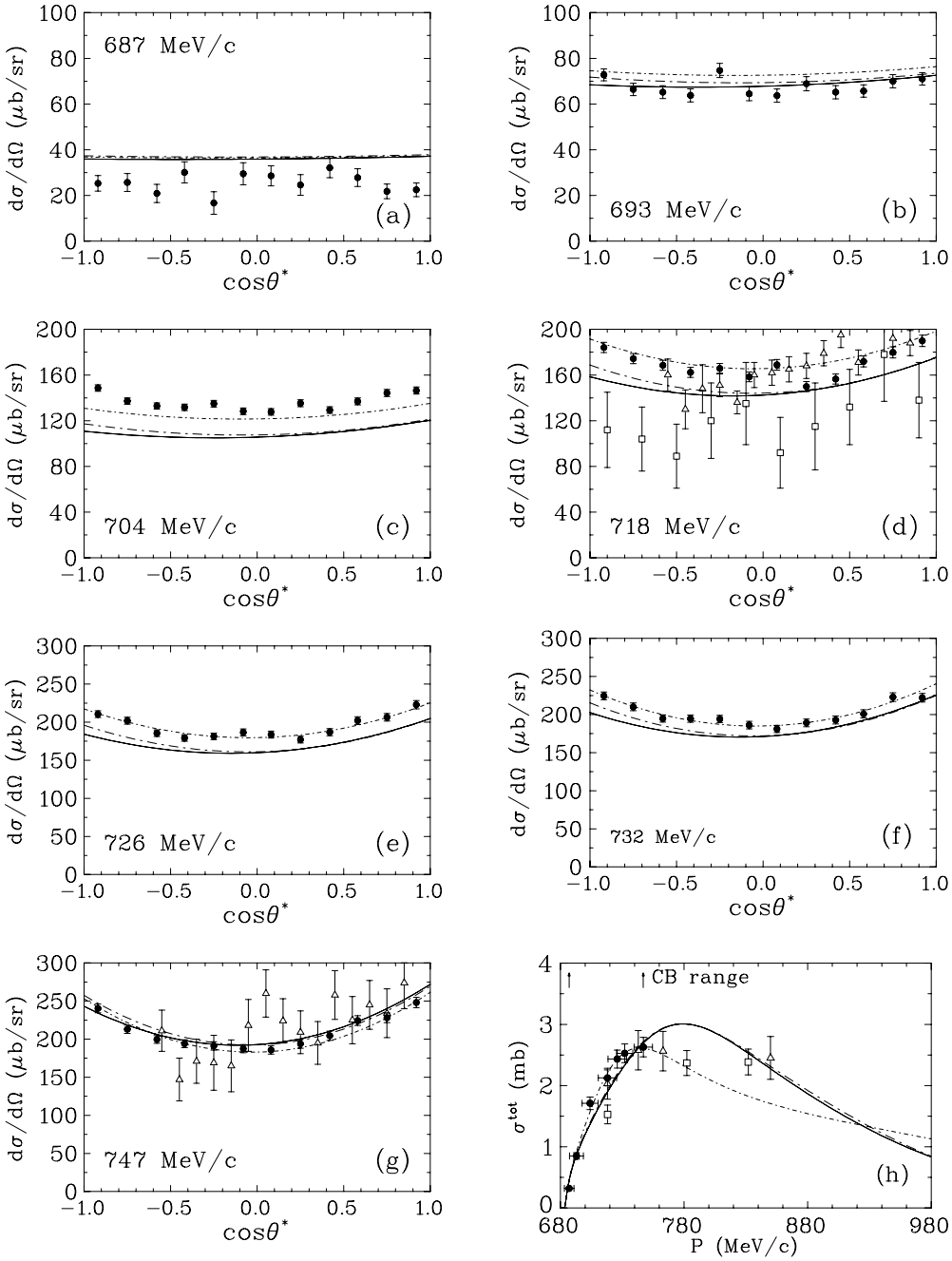

FIG. 7. (a)–(g) Differential cross section for $\pi^- p \to \eta n$ at our seven incident π^- momenta. The uncertainties are statistical only. (h) The total cross section as a function of the p_{π^-} momentum; statistical and systematical uncertainties have been combined in quadrature. The beam momentum spread is also included in the horizontal error. The FA02 [14], I375, and F375 PWA solutions described in the text are shown as solid, long-dash-dotted, and short-dash-dotted lines, respectively. Data sources are given in the legend to Fig. 6.

case by as much as 30 MeV and that the width is likely narrower as well. Definite, numerical conclusions await new data at higher energies. The D_{13} amplitude for $\pi^- N \to \eta N$ is shown in Fig. 10(b).

VI. COMPARISON OF THRESHOLD η PRODUCTION BY π^-, K^-, AND γ

The gross features of η production by π^- and K^- provide the input needed to investigate the applicability of dynamical $SU(3)$ flavor symmetry (FS), which is broken in nature. Like the related symmetry of isospin, $SU(3)$ FS is a property of massless quantum chromodynamics (QCD). For the case of η production FS results in the following relation:

$$d\sigma(\pi^- p \to \eta n)/\Phi_\pi = d\sigma(K^- p \to \eta \Lambda)/\Phi_K, \qquad (6)$$

where Φ is the density of states and Clebsch-Gordan coefficient. When the quarks are endowed with their current mass, FS

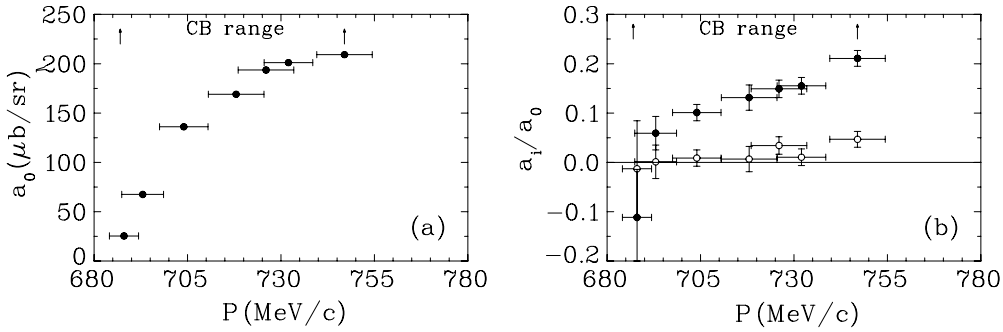

FIG. 8. Momentum dependency of (a) the a_0 coefficient of a Legendre polynomial expansion of the differential cross section, Eq. (7), (b) ratio of the coefficients a_1/a_0 (open circle) and a_2/a_0 (filled circle). The horizontal errors include the ± 2.5 MeV/c beam momentum uncertainty and the beam momentum spread.

must be broken but it is not rendered useless. The consequences of the quarks having mass are as follows:

(a) It adds the mass term $\mathcal{L}_m$ to the massless Lagrangian $\mathcal{L}_0$, see Ref. [11]. The full QCD Lagrangian $\mathcal{L}_{\rm QCD}$ is as follows:

$$\mathcal{L}_{\rm QCD} = \mathcal{L}_0 + \mathcal{L}_m.$$

The structure of this mass term is simple: $\mathcal{L}_m = \bar{q} m_q q$, where q is the quark field and m_q is the current quark mass. In general, $\mathcal{L}_m$ does not affect the dynamics of a reaction generated by $\mathcal{L}_0$ except for particle mixing.

(b) When the quarks are given their mass, that modifies the reaction kinematics and reduces the phase space, though it is not likely to lead to new dynamical effects.

Thus, the various features that we have observed in the total cross section and differential cross-section dependences in $\pi^- p \to \eta n$ are expected to be seen also in $K^- p \to \eta\Lambda$. These include (i) the immediate, strong onset of $\sigma^{\rm tot}$ upon crossing the η threshold and (ii) near threshold $\sigma^{\rm tot}$ is S wave dominated; thus $\sigma^{\rm tot}$ should increase linearly with the η c.m. momentum, p^*_η, as $\sigma^{\rm tot} = C p^*_\eta$. Our data up to $p^*_\eta = 90$ MeV/c give $C_\pi = (18 \pm 2)\mu$b/MeV/c, whereas for $K^- p \to \eta\Lambda$, the data of Ref. [4] yield $C_K = (17 \pm 3)\mu$b/MeV/c. Shown in Fig. 11 is the p^*_η dependence of $\sigma^{\rm tot}(\pi^- p \to \eta n)$ and $\sigma^{\rm tot}(K^- p \to \eta\Lambda)$.

The solid line is the prediction for $\sigma^{\rm tot}(\pi^- p \to \eta n)$ from the GW SAID FA02 analysis [14]. The data points have not been enlarged to account for the 6% systematic uncertainty in the cross section. The 2.5 MeV/c uncertainty in the absolute value of the π^- beam momenta and the beam-momentum bite are converted to uncertainty in p^*_η. These uncertainties are adequate for the data points with error bars to lie on a straight line that goes through the origin.

(c) There is no evidence for a P-wave contribution. All angular distributions are symmetric at about 90°.

(d) The angular distributions for $p_{\pi^-} > 10$ MeV/c above threshold have a bowl shape, indicative of a modest ($\lesssim$10%) D-wave contribution and S-D interference.

All four distinct features of $\pi^- p \to \eta n$ are also seen in $K^- p \to \eta\Lambda$, as reported in Ref. [4]. This provides substantial support for the manifestation of dynamical $SU(3)$ FS. We also infer that the FS breaking because of the finite quark mass is not serious in well-chosen cases. $SU(3)$ FS is an important feature for probing the (average) quark structure of baryons related by $SU(3)$. Pentaquarks and meson-baryon bound states do not exhibit $SU(3)$ FS.

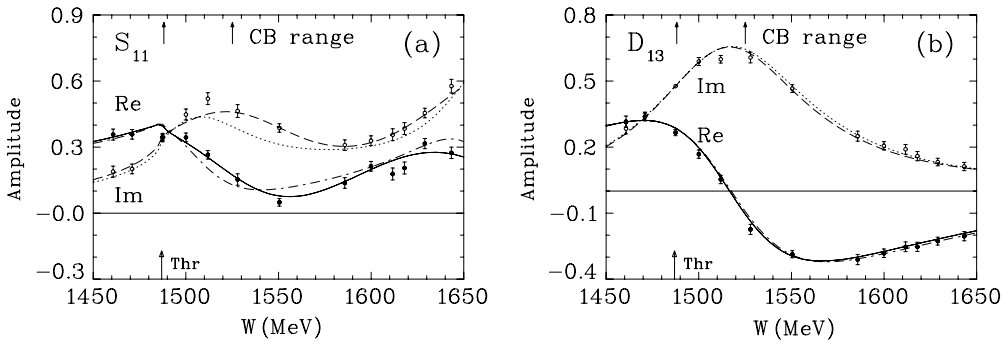

FIG. 9. (a) S_{11} and (b) D_{13} partial amplitudes for πN elastic scattering. Solid (dashed) curves give the real (imaginary) parts of amplitudes corresponding to the predictions of solution FA02 [14] (present data not included). Dash-dotted (dotted) curves show the real (imaginary) parts of amplitudes corresponding to the "forced" fit (F375). Single-energy solutions associated with FA02 solution are plotted as filled and open circles. The curves associated with solution I375 are virtually indistinguishable from FA02. All amplitudes are dimensionless.

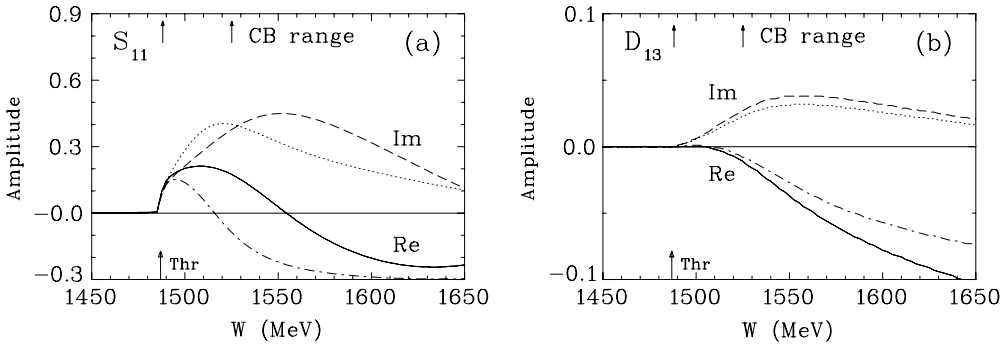

FIG. 10. (a) S_{11} and (b) D_{13} partial-wave amplitude for $\pi^- N \to \eta N$. Notation is given in the legend to Fig. 9.

We conclude with a brief comparison of η production by π^- with η photoproduction. Because the latter is an electromagnetic process, FS does not apply, and a cross-section relation, such as Eq. (6), is not to be found on the basis of symmetry. However, both η-production reactions occur predominantly by s-channel production via $N(1535)\frac{1}{2}^-$, which makes us venture that photoproduction is of order α times the π^- production and has similar p_η^* dependence

$$\sigma^{\rm tot}(\gamma p \to \eta p)/\Phi_\gamma \approx \alpha \cdot \sigma^{\rm tot}(\pi^- p \to \eta n)/\Phi_\pi. \quad (7)$$

Shown in Fig. 11 is $137\sigma^{\rm tot}(\gamma p \to \eta p)$, Ref. [6]. The p_η^* dependence is comparable for η production by π^-, K^-, and γ. The fact that the proportionality factor of 137 makes the total cross section of photoproduction agree with η production by π^- is of course fortuitous. The angular distribution $d\sigma/d\Omega(\gamma p \to \eta p)$ [6] is rather interesting; it has the shape of an inverted bowl, whereas $d\sigma(\pi^- p \to \eta n)$ is bowl shaped.

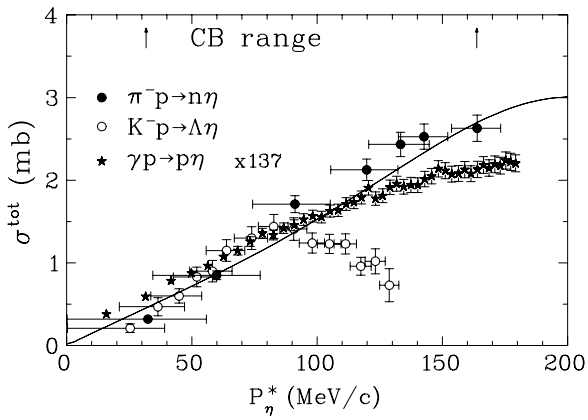

FIG. 11. p_η^* dependence of $\sigma^{\rm tot}(\pi^- p \to \eta n)$, $\sigma^{\rm tot}(K^- p \to \eta\Lambda)$, and $\sigma^{\rm tot}(\gamma p \to \eta p)$. Experimental data for $\pi^- p \to \eta n$ are from the current measurements (filled circles), data for $K^- p \to \eta\Lambda$ from [4] (open circles), and data for $\gamma p \to \eta p$ from [6] (asterisk) are multiplied by factor 137. FA02 [14] predictions for the $\pi^- p \to \eta n$ shown by the solid line. The horizontal errors for CB data include the ± 2.5 MeV/c beam momentum uncertainty and the beam momentum spread. The vertical errors for $\sigma^{\rm tot}(\pi^- p \to \eta n)$ include the 6% systematic uncertainty.

VII. SUMMARY

We have measured the differential cross section for $\pi^- p \to \eta n$ at seven incident π^- beam momenta from threshold to $p_{\pi^-} = 747$ MeV/c using the Crystal Ball multiphoton spectrometer for 12 contiguous angular intervals from $\theta^* = 0^\circ$ to 180°. The total cross section $\sigma^{\rm tot}$ was obtained by integration of $d\sigma/d\Omega$. The remarkable features of our $\pi^- p \to \eta n$ data are as follows:

(a) $\sigma^{\rm tot}(\pi^- p \to \eta n)$ increases immediately and rapidly from the η threshold at $p_{\pi^-} = 685$ MeV/c, reaching 2.6 mb at $p_{\pi^-} = 747$ MeV/c.

(b) $\sigma^{\rm tot} = (18 \pm 2) p_\eta^* \mu$b/MeV/$c$ up to $p_\eta^* \approx 90$ MeV/c. The behavior of $\sigma^{\rm tot}$ as function of p_η^* is indicative of S-wave production dominance.

(c) The $d\sigma/d\Omega$ angular distributions for $p_{\pi^-} > 704$ MeV/c are bowl shaped. This is consistent with no P-wave and a modest D-wave production of order 5–10% and S-D interference.

(d) The GW SAID FA02 prediction based on a coupled-channel analysis of πN elastic and ηn production data provides a good description of the shape of the angular distributions. The agreement with the absolute normalization could be better.

(e) There is a remarkable similarity in the features of η production by π^- and K^-. This is understood as a consequence of dynamical $SU(3)$ FS without the need for explicit quark mass corrections.

(f) A comparison of $\pi^- p \to \eta n$ with $\gamma p \to \eta p$ shows that up to $p_\eta^* \approx 120$ MeV/c, $\sigma^{\rm tot}(\pi^- p \to \eta n) \approx 137\sigma^{\rm tot}(\gamma p \to \eta p)$.

(g) The η photoproduction angular distributions are different from $\pi^- p \to \eta n$; they have opposite curvature.

ACKNOWLEDGMENTS

We gratefully acknowledge the loan of the Crystal Ball detector by SLAC. The assistance with the installation of the set up provided by AGS and BNL is much appreciated. This work was supported in part by DOE, NSF, NSERC (Canada), and RMES (Russia).

[1] M. Clajus and B. M. K. Nefkens, πN Newslett. **7**, 76 (1992).
[2] S. Prakhov *et al*. (Crystal Ball Collaboration), Phys. Rev. C **69**, 045202 (2004).
[3] L. Ya. Glozman and D. O. Riska, Phys. Rep. **268**, 263 (1996).
[4] A. Starostin *et al*. (Crystal Ball Collaboration), Phys. Rev. C **64**, 055205 (2001).
[5] B. M. K. Nefkens *et al*., *Proceedings of the Workshop on the Physics of Excited Nucleons (NSTAR2001)*, Mainz, Germany, 2001 (World Scientific, Singapore, 2001), p. 427.
[6] B. Krusche *et al*., Phys. Rev. Lett. **74**, 3736 (1995).
[7] B. Krusche and S. Schadmand, Prog. Part. Nucl. Phys. **51**, 399 (2003).
[8] W. B. Tippens *et al*. (Crystal Ball Collaboration), Phys. Rev. Lett. **87**, 192001 (2001).
[9] A. Starostin *et al*. (Crystal Ball Collaboration), Phys. Rev. C **67**, 068201 (2003).
[10] R. Abegg *et al*., Phys. Rev. D **53**, 11 (1996).
[11] S. Eidelman *et al*. (Particle Data Group), Phys. Lett. **B592**, 1 (2004).
[12] V. Crede *et al*., Phys. Rev. Lett. **94**, 012004 (2005).
[13] N. G. Kozlenko *et al*., Yad. Fiz. **66**, 112 (2003) [Phys. Atom. Nucl. **66**, 110 (2003)].
[14] R. A. Arndt, W. J. Briscoe, I. I. Strakovsky, R. L. Workman, and M. M. Pavan, Phys. Rev. C **69**, 035213 (2004).
[15] W. T. Chiang, S. N. Yang, L. Tiator, and D. Drechsel, Nucl. Phys. **A700**, 429 (2002).
[16] S. Capstick and W. Roberts, Phys. Rev. D **49**, 4570 (1994).
[17] F. Plouin *et al*., Phys. Lett. **B276**, 526 (1992).
[18] A. Lai *et al*. (NA48 Collaboration), Phys. Lett. **B533**, 196 (2002).
[19] W. Deinet *et al*., Nucl. Phys. **B11**, 495 (1969).
[20] W. B. Richards *et al*., Phys. Rev. D **1**, 10 (1970).